Solvothermal Synthesis, Crystal Structure and Photocurrent Property of a Ti_6-Core-based Titanium Oxo Cluster①

GUO Yu-Hua[a] YU You-Zhu[a②] NIU Yong-Sheng[a]
WANG Zhen[a] SHI Wei-Yun[a] WU Xian-Li[b]

[a] (*Henan Joint International Research Laboratory of Nanocomposite Sensing Materials, School of Chemical and Environmental Engineering, Anyang Institute of Technology, Anyang* 455000, *China*)

[b] (*College of Chemistry and Molecular Engineering, Zhengzhou University, Zhengzhou* 450001, *China*)

ABSTRACT A Ti_6-core-based titanium oxo cluster (TOC) $[Ti_6(\mu_2\text{-}O)_2(\mu_3\text{-}O)_2(Bpo)_2(PhCOO)_8(OiPr)_4]$ assembled by 2,2′-biphenol (H_2Bpo) and benzoic acid has been synthesized and characterized by IR, elemental analyses, thermogravimetric analysis and X-ray diffraction technique. Single-crystal X-ray diffraction analysis revealed that the complex crystallizes in monoclinic system, space group $P2_1/n$. The structure contains two $Ti_3(\mu_3\text{-}O)$ units featuring a flat mode as building blocks. Solid-state UV/Vis absorption spectrum reveals that complex **1** shows a wide range from 240 to 650 nm. Moreover, the optical band gap of **1** is estimated to be 2.35 eV. Additionally, the Ti_6-TOC exhibits good photocurrent response.

Keywords: titanium oxo cluster, crystal structure, band gap, photocurrent response;
DOI: 10.14102/j.cnki.0254–5861.2011–2921

1 INTRODUCTION

The semiconductor materials-based photocatalysts have attracted much attention due to their applications in the fields of energy and environment[1-4]. Titanium dioxide (TiO_2) is one of the most promising photocatalysts because of its high efficiency, biocompatibility and non-toxic nature[5-8]. However, only UV-light (< 5% of the solar spectrum) can be absorbed by pristine TiO_2 due to its large band gap value (*ca*. 3.20 eV), which greatly inhibits its application for photocatalysis[9-11]. Sensitizing TiO_2 by chromophore ligands may efficiently reduce its band gap value and enlarged its light absorption to Vis-light region[12, 13]. Despite advantages of the sensitized TiO_2 materials, it is still a long-term challenge to illustrate the sensitized mechanisms and structure-property relationships because of their inhomogeneous and imprecise characteristics[14, 15].

Titanium oxo clusters (TOCs) are the ideal structure and reaction models for TiO_2 which have drawn wide attention in the very recent years[16-18]. Though a large number of TOCs and metal-doped TOCs have been reported, the investigations and studies on the Ti-based complex are still less than other transitional metal-based complex. On the other hand, the chromophore ligands-based TOCs with narrow band gap values are also insufficiently among the reported TOCs, especially for band gap engineering study of TiO_2 and TOCs[16, 19]. As is well known, TOCs with narrow band gap values can always be obtained by using the phenolic ligands[20]. For example, phenol and catechol are usually used as chromophore ligands to construct TOCs featuring narrow band gap values[21, 22]. While as for H_2Bpo, it is not easy to predict the structures of TOCs because of the rotatability of the bond axis between benzene rings. Taking account of the above, it is appealing to construct TOCs using H_2Bpo as chromophore ligands. In this work, the solvothermal reactions of H_2Bpo and benzoic acid with $Ti(OiPr)_4$ in mixed organic solvent at 80 ℃ gave rise to a new Ti_6-core-based TOCs, namely $[Ti_6(\mu_2\text{-}O)_2(\mu_3\text{-}O)_2(Bpo)_2(Ba)_8(OiPr)_4]$ (**1**). Additionally, the band gap and photocurrent response property of **1** were also investigated.

2 EXPERIMENTAL

Received 28 June 2020; accepted 11 August 2020 (**CCDC 2011093**)

① This work was financially supported by the National Natural Science Foundation of China (No. 21702005), the Foundation of the Henan Joint International Research Laboratory of Nanocomposite Sensing Materials and the Foundation of Anyang Institute of Technology (YPY2019003)

② Corresponding author. Yu You-Zhu, born in 1978, professor, majoring in coordination chemistry. E-mail: 119yyz@163.com

2. 1 Materials and general methods

All starting reagents of AR grade were commercially purchased and used without further purification. The crystal data were collected on a Bruker Apex II CCD diffractometer. IR spectrum was determined on a Tensor 27 OPUS (Bruker) FT-IR spectrometer with KBr pellets in the range of 4000～400 cm^{-1}. Analyses of C and H were recorded on a Perkin-Elmer 240 Elemental analyzer. The powder X-ray diffraction patterns (PXRD) were performed on a Rigaku D/Max-2500 diffractometer at 40 kV and 100 mA, using a graphite-monochromator and a Cu-target tube under ambient conditions. Thermogravimetric analysis (TGA) experiments were recorded on a NETZSCH STA 449F3 thermal analyzer at a heating rate of 10 ℃/min from 40 to 800 ℃ under N_2. The solid UV/Vis spectra were measured on a UV25500 UV-VIS-NIR Spectrophotometer (Shimadzu Corp.).

The electrochemical measurement electrode of complex **1** was prepared by a solution coating method. Generally, the grinded crystals (5 mg) were ultrasonically dispersed in 100 uL ethanol and 10 uL Nafion solutions (5 wt%, Sigma-Aldrich). After 10 min, 40 uL suspensions were dropped on the cleaned ITO glass (1 cm^2 area) by pipette. After evaporation under ambient atmosphere for 2 hours the coating film was obtained and used as the working electrode. Photocurrent measurements and electrochemical impedance spectroscopy were conducted using CHI 760E electrochemical workstation in a three-electrode system, using a Pt plate as the auxiliary electrode and an Ag/AgCl electrode as the reference electrode. All the tests were performed at the same bias potential of +0.4 V and an aqueous solution of Na_2SO_4 (0.2 mol·L^{-1}) was used as the electrolyte. A 300 W high-pressure xenon lamp was used as a full-wavelength light source located 20 cm away from the ITO electrode, and the on-off cycling irradiation intervals are 10 s.

2. 2 Synthesis of $[Ti_6(\mu_2\text{-}O)_2(\mu_3\text{-}O)_2(Bpo)_2(PhCOO)_8(OiPr)_4]$ (1)

H_2Bpo (186 mg, 1 mmol), benzoic acid (611 mg, 5 mmol) and $Ti(OiPr)_4$ (0.5 mL, 1.5 mmol) were added with stirring to isopropanol (1 mL) and acetonitrile (5 mL). After 5 min, the resulting mixture was sealed in a Teflon-lined stainless vessel (15 mL) and heated at 80 ℃ for 36 h under autogenous pressure. The vessel was then cooled by air cooling to room temperature spontaneously. Orange-red and block single crystals were obtained by filtration, washed with acetonitrile, and dried in air. Yield: 0.255 g (53%, based on $Ti(OiPr)_4$). Elemental analysis: calcd. (found) for $C_{92}H_{84}O_{28}Ti_6$ (%): C, 57.41(57.29); H, 4.40(4.35). IR (KBr, cm^{-1}): 3062(w), 2971(w), 2927(w), 2888(w), 1595(s), 1550(s), 1490(m), 1419(s), 1269(s), 1126(s), 1020(s), 717(s), 678(m), 642(s), 605(s) and 482(s).

2. 3 Crystallographic measurements and structure determination

The suitable single crystal of complex **1** used for X-ray diffraction experiment was obtained directly from the above experiment. Crystallographic data of **1** were collected at room temperature on a Bruker APEX II diffractometer by using an ω-2θ scan mode. The X-ray source is a graphite-monochromatized Mo$K\alpha$ radiation (λ = 0.71073 Å). The structure was solved by direct methods using the SHELXS-97 programs[23] and refined by full-matrix least-squares on F^2 using the SHELXL-2014 program package[24]. The non-hydrogen atoms were refined anisotropically, and the hydrogen atoms were added theoretically, riding on the concerned atoms and refined with fixed thermal factors. Crystal data for **1**: monoclinic system, space group $P2_1/n$ with a = 13.8085(6), b = 16.5884(9), c = 20.5623(14) Å, β = 99.502(5)°, V = 4645.4(5) $Å^3$, Z = 2, $C_{92}H_{84}O_{28}Ti_6$, M_r = 1924.99, D_c = 1.376 g/cm^3, F(000) = 1984, $GOOF$ = 1.076, the final R = 0.0796, wR = 0.1482 ($w = 1/[\sigma^2(F_o^2) + (0.0720P)^2 + 4.06P]$, where $P = (F_o^2 + 2F_c^2)/3$), $(\Delta\rho)_{max}$ = 0.744 and $(\Delta\rho)_{min}$ = –0.521 e/$Å^3$. The selected bond lengths and bond angles and the hydrogen bond information for **1** are given in Table 1.

Table 1. Selected Bond Lengths (Å) and Bond Angles (°) for 1

Bond	Dist.	Bond	Dist.
Ti(1)–O(8)	1.738(3)	Ti(2)–O(9)	2.107(3)
Ti(1)–O(11)	2.016(3)	Ti(2)–O(10)	2.092(3)
Ti(1)–O(12)	2.023(3)	Ti(2)–O(8)	1.896(3)
Ti(1)–O(13)	1.995(3)	Ti(3)–O(5)	2.035(3)
Ti(1)–O(2)#1	2.119(3)	Ti(3)–O(3)	1.854(3)
Ti(1)–O(5)#1	1.922(3)	Ti(3)–O(4)	2.001(3)
Ti(2)–O(5)	1.912(3)	Ti(3)–O(2)	1.983(3)
Ti(2)–O(6)	2.043(3)	Ti(3)–O(1)	1.748(3)
Ti(2)–O(7)	1.738(3)	Ti(3)–O(14)#1	2.154(3)

To be continued

Angle	(°)	Angle	(°)
O(8)–Ti(1)–O(2)#1	176.73(11)	O(1)–Ti(3)–O(4)	92.94(15)
O(8)–Ti(1)–O(5)#1	105.78(12)	O(1)–Ti(3)–O(5)	100.12(15)
O(8)–Ti(1)–O(11)	91.72(12)	O(1)–Ti(3)–O(14)#1	174.23(14)
O(5)–Ti(2)–O(6)	92.35(12)	O(3)–Ti(3)–O(2)	89.52(13)
O(5)–Ti(2)–O(9)	86.32(12)	O(3)–Ti(3)–O(4)	97.09(14)
O(5)–Ti(2)–O(10)	168.66(13)	O(3)–Ti(3)–O(5)	160.05(14)
O(6)–Ti(2)–O(9)	81.75(13)	O(4)–Ti(3)–O(5)	92.01(12)
O(1)–Ti(3)–O(2)	99.76(14)	O(4)–Ti(3)–O(14)#1	81.30(13)
O(1)–Ti(3)–O(3)	97.11(17)	O(5)–Ti(3)–O(14)#1	80.45(12)

Symmetry code: #1 –*x* + 1, –*y* + 1, –*z* + 1

3 RESULTS AND DISCUSSION

3. 1 Description of the crystal structure

Complex **1** crystallizes in monoclinic system, space group $P2_1/n$. The crystal structure of complex **1** is revealed in Fig. 1a and b, and the stacking structure is shown in Fig. 2. As shown in Fig. 1a, complex **1** consists of six Ti^{4+} ions, two μ_2-O ions, two μ_3-O ions, two Bpo anions, eight benzoates and four isopropoxide groups. All Ti^{4+} ions show octahedral TiO_6 coordination environments. Two edge-sharing Ti^{4+} ions are linked by one μ_3-O and one μ_2-O atom which can generate a Ti_2 subunit, then the Ti_2 subunits and another Ti^{4+} ion linked by one μ_3-O can generate a Ti_3O subunit featuring a nearly flat mode by vertex-sharing mode. Finally, the two Ti_3O subunits are connected by two μ_2-O atoms via vertex-sharing mode to form a Ti_6 core structure (Fig. 1b). In complex **1**, the substitued ratio of PhCOO:Ti is 4:3 which is a higher degree than most of the reported Ti_6 cores-based TOCs. In addition, the average bond lengths of Ti1–O, Ti(2)–O and Ti(3)–O in **1** are 1.969, 1.965 and 1.963 Å respectively, which are consistent with the literature[11, 16, 21]. Notably, the Bpo anions as CLs ligand in complex **1** make its crystals orange red.

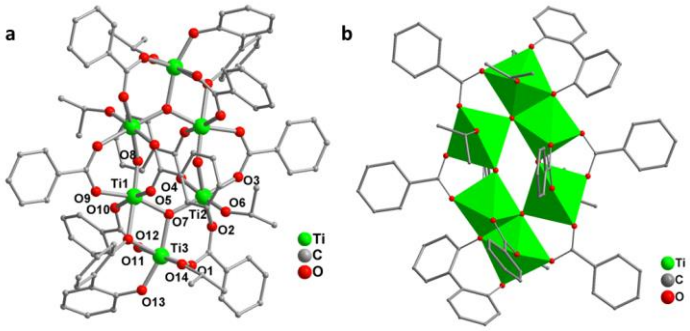

Fig. 1. Ball-stick (a) and polyhedral (b) views for the structure of 1. The H atoms have been omitted for clarity

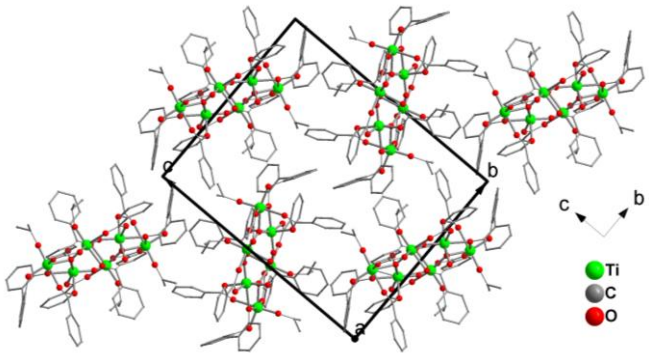

Fig. 2. Stacking structure of complex 1 (view along axis *a*). All H atoms are omitted for clarity

3. 2 IR spectrum

The absorption peak at 3062 cm^{-1} should be assigned to the stretching vibrations of the C–H bonds of benzenes. The peaks at 2971, 2927 and 2888 cm^{-1} can be ascribed to the stretching vibration of the saturated C–H bonds, whereas peaks at 1595, 1550 and 1490 cm^{-1} could be assigned to the vibration of benzene rings. Notably, the characteristic sharp vibrations of the Ti-OR bands are in the region of 400～750 nm, whereas the peaks at 1126 and 1020 cm^{-1} can be ascribed to the vibration of TiO-C bonds[25].

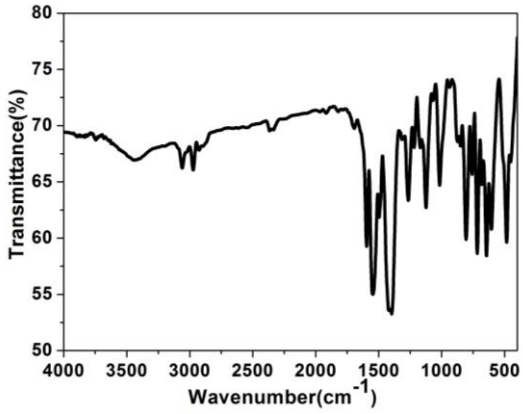

Fig. 3. Simulated and experimental PXRD patterns for complex 1

3. 3 Powder X-ray diffraction (PXRD) and thermal stability

The pure phase of complex **1** was confirmed by the powder X-ray diffraction performed at room temperature. As shown in Fig. 4, the RXPD experimental pattern was in good agreement with the computer-simulated pattern, which confirmed the pure phase of **1**. The different intensities of reflections between the experimental and simulated patterns are mostly because of the powder size and variation in preferred orientation of the powder samples during the collection of experimental PXRD data.

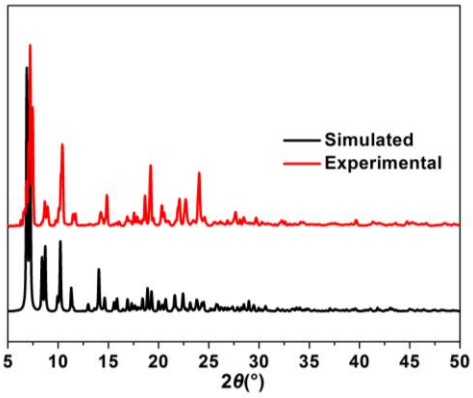

Fig. 4. Simulated and experimental PXRD patterns for complex 1

The thermogravimetric analysis (TGA) of complex **1** was also performed. As shown in Fig. 5, complex **1** shows thermal stability under 200 ℃. It can be observed that the obvious weight loss step is in the range of 250～500 ℃ with the weight loss of about 64.07%, which can be ascribed to the release of organic ligands. Then, the last residue remains about 28.24% at 800 ℃.

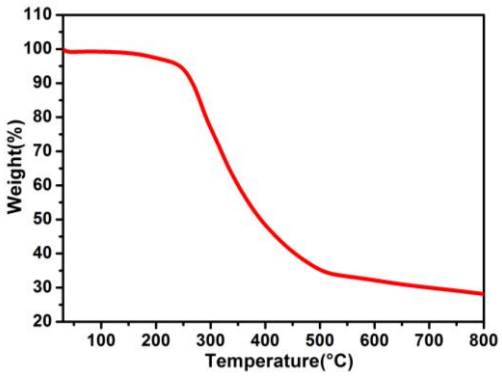

Fig. 5. TGA curve of complex 1

3. 4 Diffuse-reflectance UV-Vis spectra and photoluminescence properties

Solid-state UV/Vis absorption spectrum of complex **1** was measured at room temperature using $BaSO_4$ as a standard reference (Fig. 6a). Complex **1** shows a wide absorption range from λ = 240 to 650 nm. The absorption range from 240 to 400 nm could be ascribed to the aromatic ligands and the Ti oxo cores, whereas the absorption range from 400 to 650 nm should be mainly affected by the chromophore ligands in the structure. To be noted, the wide absorption range of complex **1** from UV to Vis-light region may greatly improve its photo-absorption efficiency for photocatalysis application. According to the Kubelka-Munk function method[18, 26], the optical band gap of complex **1** is estimated to be 2.35 eV from the solid-state UV/Vis reflection spectrum (Fig. 6b), which is a larger decrease than that of TiO_2.

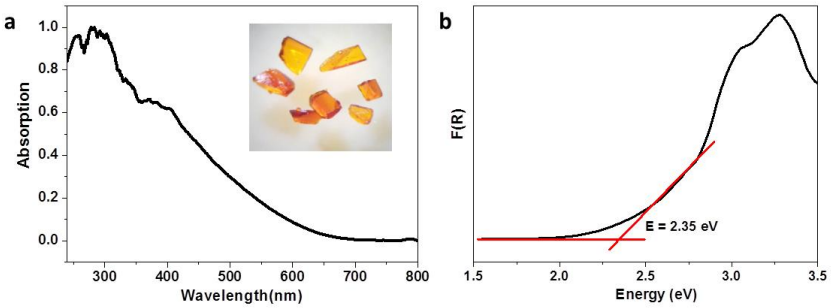

Fig. 6. Solid-state UV/Vis absorption (a) and band gap (b) of complex 1

As shown in Fig. 7a, the electrochemical impedance spectroscopy (EIS) of complex **1** has been carried out to evaluate its charge transfer resistance. The small semicircle of complex **1** in the high frequency range indicates its small charge transfer resistance. The charge-separation efficiency of semiconductor material is also very important for their photocatalytic reaction. The transient short-circuit photocurrent test of complex **1** has been carried out. As shown in Fig. 7b, complex **1** showed clear photocurrent response property. Obviously, the photocurrent was quickly generated with the light on, and the photocurrents rapidly decayed with the light off. The photocurrent density of complex **1** is about 0.062 μA cm^{-2}, which is nearly correspondent with 0.08 μA cm^{-2} of the same type of complex[16].

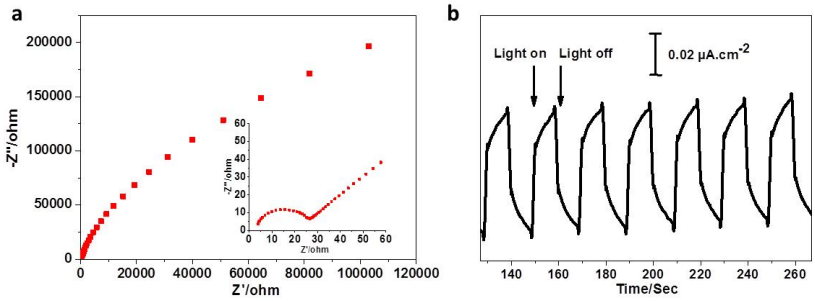

Fig. 7. Nyquist plot (a) and photocurrent response under repetitive irradiation (b) of complex 1

4 CONCLUSION

In conclusion, by the application of H_2Bpo and benzoic acid, we successfully synthesized a Ti_6-core-based TOC in a simple and general approach. The title complex shows a wide light-absorption range of 240 to 650 nm and a narrow band gap value of 2.35 eV. The charge transfer resistance and photocurrent response were also investigated. This work may not only enrich the family of TOCs but also provide important information for sensitized method of TiO_2.

REFERENCES

(1) Wadia, C.; Alivisatos, A. P.; Kammen, D. M. Materials availability expands the opportunity for large-scale photovoltaics deployment. *Energy Environ. Sci*. **2009**, 43, 2072–2077.

(2) Liu, S.; Tang, Z. R.; Sun, Y.; Colmenares, J. C.; Xu, Y. J. One-dimension-based spatially ordered architectures for solar energy conversion. *Chem. Soc. Rev*. **2015**, 44, 5053–5075.

(3) Singh, A. K.; Montoya, J. H.; Gregoire, J. M.; Persson, K. A. Robust and synthesizable photocatalysts for CO_2 reduction: a data-driven materials discovery. *Nat. Commun*. **2019**, 10, 1–9.

(4) Kuehnel, M. F.; Orchard, K. L.; Dalle, K. E.; Reisner, E. Selective photocatalytic CO_2 reduction in water through anchoring of a molecular Ni catalyst on CdS nanocrystals. *J. Am. Chem. Soc.* **2017**, 139, 7217–7223.

(5) Kongkanand, A.; Tvrdy, K.; Takechi, K.; Kuno, M.; Kamat, P. V. Quantum dot solar cells. Tuning photoresponse through size and shape control of CdSe-TiO_2 architecture. *J. Am. Chem. Soc.* **2008**, 130, 4007–4015.

(6) Yu, J.; Low, J.; Xiao, W.; Zhou, P.; Jaroniec, M. Enhanced photocatalytic CO_2-reduction activity of anatase TiO_2 by coexposed {001} and {101} facets. *J. Am. Chem. Soc.* **2014**, 136, 8839–8842.

(7) Guan, G. Q.; Zou, M. Z.; Lin, J. P.; Yan, G. Y. Annealing temperature effects of TiO_2 nanofiber anodes for the rechargeable lithium ion batteries. *Chin. J. Struct. Chem*. **2017**, 36, 729–737.

(8) Shen, S. F.; Qian, K. T.; Chen, J. P.; Wen, M. Y. One-step growth of hierarchical nanotreelike TiO_2 on ITO without template and its application in gas sensor. *Chin. J. Struct. Chem*. **2019**, 38, 1743–1751.

(9) Xu, X.; Randorn, C.; Efstathiou, P.; Irvine, J. T. A red metallic oxide photocatalyst. *Nat. Mater*. **2012**, 11, 595.

(10) Wang, C.; Liu, C.; Tian, H. R.; Li, L. J.; Sun, Z. M. Designed cluster assembly of multidimensional titanium coordination polymers: syntheses, crystal structure and properties. *Chem.-Eur. J.* **2018**, 24, 2952–2961.

(11) Yu, Y. Z.; Guo, Y.; Zhang, Y. R.; Liu, M. M.; Feng, Y. R.; Geng, C. H.; Zhang, X. M. A series of silver doped butterfly-like Ti_8Ag_2 clusters with two Ag ions panelled on a Ti_8 surface. *Dalton Trans*. **2019**, 48, 13423–13429.

(12) Pelaez, M.; Nolan, N. T.; Pillai, S. C.; Seery, M. K.; Falaras, P.; Kontos, A. G.; Dunlop, P. S.; Hamilton, J. W.; Byrne, J. A.; O'shea, K. A review on the visible light active titanium dioxide photocatalysts for environmental applications. *Appl. Catal., B* **2012**, 125, 331–349.

(13) Benkstein, K. D.; Kopidakis, N.; Van de Lagemaat, J.; Frank, A. Influence of the percolation network geometry on electron transport in dye-sensitized titanium dioxide solar cells. *J. Phys. Chem. B* **2003**, 107, 7759–7767.

(14) Labat, F.; Le Bahers, T.; Ciofini, I.; Adamo, C. First-principles modeling of dye-sensitized solar cells: challenges and perspectives. *Acc. Chem. Res*. **2012**, 45, 1268–1277.

(15) Duncan, W. R.; Prezhdo, O. V. Temperature independence of the photoinduced electron injection in dye-sensitized TiO_2 rationalized by *ab initio* time-domain density functional theory. *J. Am. Chem. Soc.* **2008**, 130, 9756–9762.

(16) Yu, Y. Z.; Zhang, Y. R.; Geng, C. H.; Sun, L.; Guo, Y.; Feng, Y. R.; Wang, Y. X.; Zhang, X. M. Precise and wide-ranged band-gap tuning of Ti_6-core-based titanium oxo clusters by the type and number of chromophore ligands. *Inorg. Chem.* **2019**, 58, 16785–16791.

(17) Fang, W. H.; Zhang, L.; Zhang, J. Synthetic strategies, diverse structures and tuneable properties of polyoxo-titanium clusters. *Chem. Soc. Rev*. **2018**, 47, 404–421.

(18) Fang, W. H.; Zhang, L.; Zhang, J. A 3.6 nm Ti_{52}-oxo nanocluster with precise atomic structure. *J. Am. Chem. Soc.* **2016**, 138, 7480–7483.

(19) Liu, J. X.; Gao, M. Y.; Fang, W. H.; Zhang, L.; Zhang, J. Bandgap engineering of titanium-oxo clusters: labile surface sites used for ligand substitution and metal incorporation. *Angew. Chem., Int. Ed*. **2016**, 55, 5160–5165.

(20) Benedict, J. B.; Coppens, P. The crystalline nanocluster phase as a medium for structural and spectroscopic studies of light absorption of photosensitizer dyes on semiconductor surfaces. *J. Am. Chem. Soc.* **2010**, 132, 2938–2944.

(21) Narayanam, N.; Fang, W. H.; Chintakrinda, K.; Zhang, L.; Zhang, J. Deep eutectic-solvothermal synthesis of titanium-oxo clusters protected by pi-conjugated chromophores. *Chem. Commun.* **2017**, 53, 8078–8080.

(22) Lv, H. T.; Li, H. M.; Zou, G. D.; Cui, Y.; Huang, Y.; Fan, Y. Titanium-oxo clusters functionalized with catecholate-type ligands: modulating the optical properties through charge-transfer transitions. *Dalton Trans*. **2018**, 47, 8158–8163.

(23) Sheldrick, G. M. *SHELXS-97, Program for X-ray Crystal Structure Solution*. University of Göttingen, Germany **1997**.

(24) Sheldrick, G. M. Crystal structure refinement with SHELXL. *Acta Crystallogr., Sect. C: Struct. Chem*. **2015**, 71, 3−8.

(25) Soler-Illia, G. J. D. A.; Rozes, L.; Boggiano, M. K.; Sanchez, C.; Majoral, J. I. New mesotextured hybrid materials made from assemblies of dendrimers and titanium(IV)-oxo-organo clusters. *Angew. Chem., Int. Ed.* **2000**, 39, 4419–4424.

(26) Wendlandt, W. W.; Hecht, H. G. *Reflectance Spectroscopy*, Interscience, New York **1966**.